FFPI-FBG hybrid sensor to measure the thermal expansion and thermo-optical coefficient of a silica-based fiber at cryogenic temperatures

Litong Li (李立彤)[1,2,*], Dongsheng Zhang (张东生)[1], Xiaoyan Wen (文晓艳)[3], and Sisi Peng (彭思思)[4]

[1]*National Engineering Laboratory for Fiber Optic Sensing Technology, Wuhan University of Technology, Wuhan 430070, China*

[2]*Key Laboratory of Fiber Optic Sensing Technology and Information Processing, Ministry of Education, Wuhan University of Technology, Wuhan 430070, China*

[3]*School of Science, Wuhan University of Technology, Wuhan 430070, China*

[4]*Wuhan Institute of Marine Electric Propulsion, CSIC, Wuhan 430070, China*

**Corresponding author: 13163386978@163.com*

Received May 15, 2015; accepted July 23, 2015; posted online August 31, 2015

In this Letter, a sensor consisting of a fiber Bragg grating (FBG) and a fiber Fabry–Perot interferometer (FFPI) sensor is developed to measure the coefficient of thermal expansion (CTE) and the thermo-optical coefficient (TOC) of a silica-based optical fiber at cryogenic temperatures. The FFPI is fabricated by welding together two acid-etched fibers. The temperature performance of the FFPI-FBG hybrid sensor is studied in the temperature range of 30–273 K. The CTE and TOC of the optical fiber at cryogenic temperatures are derived analytically and verified by experiments.

OCIS codes: 060.2300, 060.2370, 060.2400.
doi: 10.3788/COL201513.100601.

In recent years, the fiber Bragg grating (FBG) sensor has attracted increasing attention, especially in cryogenic fields such as aerospace, large superconducting magnets, and natural gas storage and transportation. The advantages provided by the FBG sensor include its small profile, light weight, high sensitivity, and immunity to electromagnetic interference, all of which have great potential for applications in a cryogenic environment[1–3]. Extensive research on the performance of FBGs at cryogenic temperatures has been carried out. James *et al.* reported that the strain response of FBG sensors was temperature-independent and that the temperature response was nonlinear over a temperature range of 2.2–280 K[4]. Guo *et al.* reported that the cryogenic temperature performance of FBG sensors was studied in the temperature range of 123–273 K by three FBG experiments[5]. Saidi *et al.* studied the temperature response of FBGs in the temperature range from 77 to 298 K[6]. Ramalingam and Neumann also did the same test, but theirs was from room temperature falling to 77 K[7]. Based on the above works, the relationship between the wavelength shift and temperature all can be characterized by a three-order polynomial. But even in the same cryogenic environment, different researchers get different results. The physical properties and optical properties of silica at or above room temperature are well known, but the parameter at cryogenic temperatures remains unclear. Thus, the FBG sensing mechanism at normal temperatures is no longer suitable in a cryogenic environment[8]. All the research thus far has focused primarily on description of this phenomenon, but studies on the cryogenic properties of optic fibers are rarely reported. By monitoring the temperature and strain inside cryogenic equipment, such as a superconducting magnet with a FBG sensor, we should also explore the underlying cause of the wavelength change of a FBG, which is caused by either temperature or strain. However, the temperature sensitivity of a FBG is determined by the coefficient of thermal expansion (CTE) and the thermo-optical coefficient (TOC). Recently, many approaches have been reported for fiber-optic sensors for the measurement of the TOC. Kim *et al.* developed a fiber-optic interferometric probe for measuring the TOCs of liquid samples like deionized water, ethanol, and acetone[9]. The sensor was fabricated by fusion splicing a short piece of a two-mode fiber to a single-mode fiber (SMF) with a small lateral offset, which causes interference between the LP_{01} and LP_{02} modes. It could measure the temperature and TOC simultaneously by analyzing the peak position of the interference Fourier spectrum and the intensity level. Lee *et al.* also presented a microcavity fiber Fabry–Perot interferometer (FFPI) that was based on dual hollow-core fibers and could determined the TOC of liquids like deionized water and ethanol[10]. The experimental results demonstrated that the measured values deviated only by 10^{-5}–10^{-6} from the published results for the same liquids.

By combining a FBG with a FFPI sensor, this Letter proposes a method to measure the CTE and TOC of a silica-based optical fiber in the temperature range of 30–273 K. The FFPI-FBG hybrid sensor is fabricated by hydrofluoric acid (HFA) etching the SMF to form a

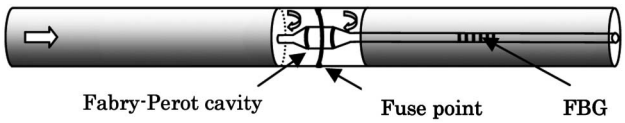

Fig. 1. Schematic structure of the FFPI-FBG hybrid sensor.

Fabry–Perot cavity in the fiber and fusing it with a FBG. When the FFPI-FBG hybrid sensor was moved from room temperature into the cryogenic temperature, both the wavelength of the FBG and the interference peak of the FFPI would change simultaneously[11]. By decoding and analyzing the sensor parameters, combined with the temperature change, we can calculate the two critical values at cryogenic temperatures.

As shown in Fig. 1, the specific fabrication process of the sensor is as follows: the FFPI is made from two HFA-etched SMFs and the segment near one of the SMF's end faces has a FBG.

First, we get the SMF end faces clean and flat by cutting and grinding them. The SMF employed was a fused silica HIPOSH® fiber (YOFC Ltd, China) with core/cladding of 9/125 μm. Second, the fiber end faces were immersed in a HFA solution for 2–3 min. The concentration of the HFA used in the experiments was 40%. Due to the fact that the etch rate of the fiber core is faster than that of the cladding, a hole was formed in that part of the fiber core after 2–3 min. Third, the etched fibers were cleaned thoroughly in deionized water. Finally, the two etched fibers were positioned and buttered together on a fusion splicer (Erisson Model FSU975). After fusion, the fiber's Fabry–Perot cavity was generated inline[12]. It can be seen from Fig. 2 that the cavity of the FFPI was measured to be 64.9 μm by using a digital microscope (VHX-100).

The reflective spectrum of the FFPI-FBG hybrid sensor is shown in Fig. 3. It is measured by using a high-accuracy, homemade optical spectrum analyzer (OSA) (Bayspec, USA). The acquisition rate is 2 kHz, and the wavelength resolution is 0.1 pm over a spectral range of 1265–1315 nm. When the temperature changes, the wavelength of the FBG will change and the spectrum of the FFPI will shift; then, the test parameters can be calculated[13,14].

Since the optical fiber was very thin and the sensor's tensile strength had been weakened after HFA etching and fusion splicing, we designed a method to protect the sensor during the temperature test. As shown in Fig. 4, we had removed one end fiber of the sensor and kept another end that was close to the FBG. Then, we put the sensor into a cylindrical steel tube (length 4 cm, diameter 4 mm) and fixed the end at the cutter of the metal

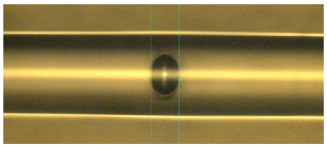

Fig. 2. Digital microscope image of the hybrid sensor.

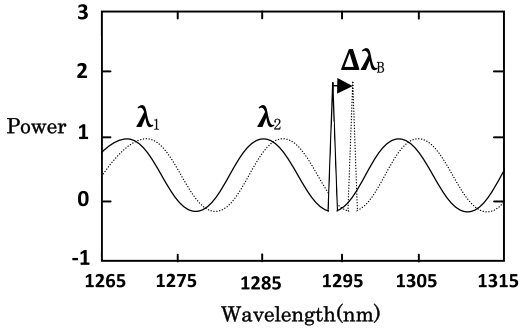

Fig. 3. Reflective spectrum of the hybrid sensor.

tube with an adhesive. This package can keep the sensor free from external forces.

With ΔT being the variation of the temperature and λ_B the center wavelength of the FBG, the temperature measuring principle of FBG is

$$\frac{\Delta\lambda_B}{\lambda_B} = (\xi + \alpha) \times \Delta T, \tag{1}$$

where ξ and α are the CTE and TOC, respectively[15].

According to the phenomenon of swelling by heat and shortening by cold, the FFPI cavity will change since the temperature changes. Thus, we can obtain

$$\Delta L = \xi L \Delta T, \tag{2}$$

where L is the cavity length of the FFPI, and ΔL is the variation caused by the temperature change.

Through peak tracking in the interference spectrum, the FFPI cavity length L was calculated from the reflective spectrum, as given by

$$L = \frac{\lambda_1 \lambda_2}{2(\lambda_2 - \lambda_1)}, \tag{3}$$

where λ_1 and λ_2 are adjacent peak points in the spectrum of the FFPI[16]. Since the wavelength precision of the OSA is 0.1 pm, from Eq. (3), we can get the minimum measured quantity of the FFPI cavity length, which is 0.0001 μm.

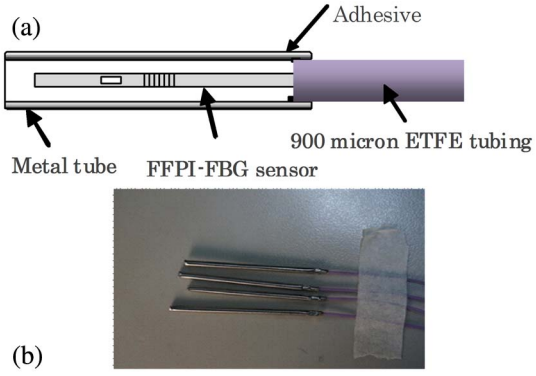

Fig. 4. (a) Configuration and (b) actual packaging of the hybrid sensor.

Thus, the CTE in different temperature ranges can be calculated using Eqs. (2) and (3). The quartz SMF is composed of core and cladding with different refractive indices. The main raw material of the SMF is fused silica, and the material composition and structure of the SMF is SiO_2-GeO_2-F. The GeO_2 is doped in the core and only F is in the cladding. But the doping concentrations must be very tiny to get the perfect viscosity match between the core and cladding. As long as the raw material is consistent and the doping amount is very tiny, combined with a good manufacturing process, the CTEs of the core and cladding can be regarded as approximately the same[17].

So, the TOC can be expressed as

$$\alpha = \frac{\Delta\lambda_B}{\lambda_B \Delta T} - \xi. \tag{4}$$

(1) The room temperature test:

For fused silica fibers at room temperature, ξ is approximately 0.5×10^{-6}/K[18], and α has been found to range between 6×10^{-6} and 7×10^{-6}/K[19,20]. To verify the performance of the FFPI-FBG hybrid sensor, room temperature experiments were carried out using a high and low temperature test chamber (TEMI300) with a temperature control accuracy of 0.01 K. The test was done at room temperature in increments of 303 K, rising to 363 K. The test was repeated thrice. The temperature responses of the FBG and FFPI are plotted in Fig. 5. The solid line is a linearly fitted curve of the average value versus the temperature. The wavelength shift and the cavity length change have shown good linearity and repeatability for temperatures rising to 363 K. A temperature sensitivity of 8.34 pm/K with a repeatability error of 0.1% for the FBG wavelength and of 3.35×10^{-5} μm/K with a repeatability error of 4% for the cavity length were obtained.

Thus, we can acquire the CTE ξ from Eq. (2),

$$\xi = \frac{\Delta L}{L \Delta T} = 5.15 \times 10^{-7} \tag{5}$$

Also, we can acquire the TOC α from Eq. (4),

$$\alpha = \frac{\Delta\lambda_B}{\lambda_B \Delta T} - \xi = 5.92 \times 10^{-6}. \tag{6}$$

The CTE is 5.15×10^{-7}/K, and the TOC is 5.92×10^{-6}/K at room temperatures, which agrees well with the theoretical values[18–20]. Thus, we can depend on the accuracy of the test data from the hybrid sensor.

(2) The cryogenic temperature test:

A schematic drawing of the cryogenic experimental setup is shown in Fig. 6. The package surface of the sensor is filled with cryogenic adhesive, and the sensor is fixed at the object stage of the cryogenic vessel to ensure the heat exchange. A Lakeshore Model 331 cryogenic thermocoupler placed near the sensor is used as a reference and for the standard temperature measurement.

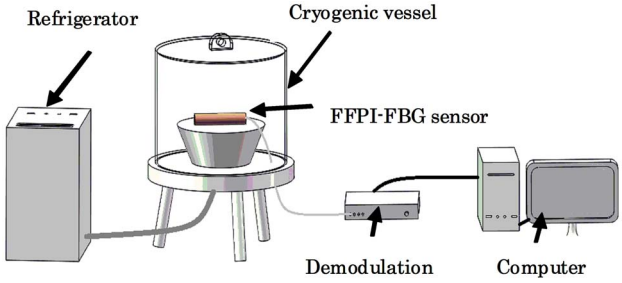

Fig. 6. Cryogenic experimental setup.

The pressure in the cryogenic vessel drops to 10^{-2} Torr through the use of a molecular vacuum pump. After about 3 h in the refrigerator, the temperature in the object stage of the cryogenic vessel drops down successfully from 273 to 30 K. When we turn the refrigerator off, the temperature will rise to room temperature from 30 K. The entire period of temperature rising lasts for 48 h. The Lakeshore Model 331 cryogenic (accuracy: 0.1 K) test system keeps a real-time record of the temperature at 1 Hz. Also, the demodulation for the FFPI-FBG sensor is set to save the data at 1 Hz. So, the temperature data and the sensor data produced time curves that mirrored each other.

The temperature responses of the FBG and FFPI are plotted in Fig. 7. The experimental data shows that this sensor has good repetition in the two periods. From the Fig. 7, it can be seen that in the cryogenic temperature test, the maximum repetition errors of the FFPI and FBG are 0.0006 μm and 20 pm, respectively. Through differential operations using Eq. (4), we can get

$$\Delta L = \frac{-\lambda_2^2}{2(\lambda_2 - \lambda_1)^2} \Delta\lambda_1, \tag{7}$$

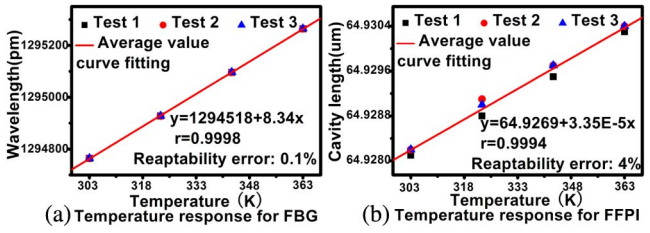

Fig. 5. Room temperature performance of the FFPI-FBG hybrid sensor.

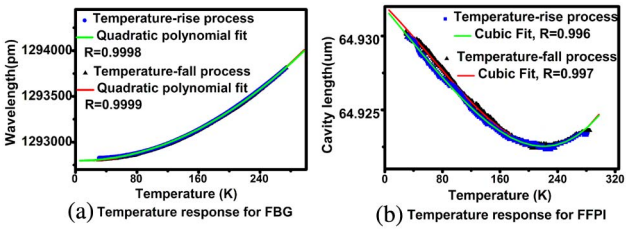

Fig. 7. (a) Bragg wavelength and (b) FFPI cavity length versus the temperature at cryogenic temperatures.

As the spectral intensity of the FFPI is weak, the peak searching for the OSA could be error prone. From Eq. (7), it can be seen that when the wavelength precision of the OSA is 0.1 pm, the test error of the FFPI is nearly 10^{-3} μm. It was assumed that the temperature fluctuation was 3 K, combined with the sensitivity of the sensor at room temperature. The corresponding test errors of the two sensors were nearly 24 pm and 10^{-3} μm. The measurement error may come from the rough, uneven surface of the FFPI micro-cavity, the temperature fluctuation during the experiment, and the measurement error of the OSA.

It is found from the Fig. 7 that the shift in the Bragg wavelength is nonlinear from 273 to 30 K. The cavity length change of the FFPI is also nonlinear during the test. For the two processes, we define the wavelength of the FBG and the cavity length of the FFPI to be the initial value when the temperature is 273 K. The red line and green line in Fig. 7(a) are the quadratic polynomial fitted curves of the Bragg wavelength versus the temperature. The red line and green line in Fig. 7(b) are the cubic polynomial fitted curves of the FFPI cavity length versus the temperature. The polynomial expression is as follows.

For the temperature-fall process:

$$\Delta\lambda_B = -1015.6 - 0.2622\,T + 0.0145\,T^2, \tag{8}$$

$$\Delta L = 0.008 - (3.97\times10^{-5})\,T - (2.03\times10^{-7})\,T^2 + (9.9\times10^{-10})\,T^3. \tag{9}$$

For the temperature-rise process:

$$\Delta\lambda_B = -1010.76 - 0.0277\,T + 0.0136\,T^2, \tag{10}$$

$$\Delta L = 0.008 - (5.78\times10^{-5})\,T - (5.09\times10^{-8})\,T^2 + (5.49\times10^{-10})\,T^3, \tag{11}$$

where T is in Kelvins.

It can be seen from Fig. 7(b) that the cavity length of the FFPI first decreases and then increases when the temperature drops. The expansivities for fused silica have negative contributions at cryogenic temperatures. The CTE of the fused silica is negative for all temperatures below approximately 220 K. This behavior is commonly attributed to the transverse thermal motion of oxygen in the Si-O-Si linkages[21,22]. As shown in Eq. (5), through differential operations in approaching the curve function, we can obtain the CTE of the fused silica.

For the temperature-fall process:

$$\xi = (0.4\times10^{-10})\,T^2 - (0.625\times10^{-8})\,T - (0.611\times10^{-6}). \tag{12}$$

For the temperature-rise process:

$$\xi = (0.253\times10^{-10})\,T^2 - (0.156\times10^{-8})\,T - (0.89\times10^{-6}). \tag{13}$$

After the average calculation of Eqs. (12) and (13), the CTE can be given by

$$\xi = (0.3265\times10^{-10})\,T^2 - (0.39\times10^{-8})\,T - (0.75\times10^{-6}). \tag{14}$$

As shown in Eq. (6), the TOC and CTE correspond to the equation as follows.

For the temperature-fall process:

$$\alpha + \xi = \frac{\Delta\lambda_B}{\lambda_B \Delta T} = (2.24\times10^{-8})\,T - (2.02\times10^{-7}). \tag{15}$$

For the temperature-rise process:

$$\alpha + \xi = \frac{\Delta\lambda_B}{\lambda_B \Delta T} = (2.1\times10^{-8})\,T - (2.14\times10^{-8}). \tag{16}$$

After the average calculation of Eqs. (15) and (16), the TOC α can be given by:

$$\alpha = (0.3265\times10^{-10})\,T^2 + (1.7795\times10^{-8})\,T - (8.615\times10^{-7}). \tag{17}$$

where T is in Kelvins and the temperature ranges from 30 to 273 K.

Leviton *et al.* had tested the TOC of fused silica (Corning 7980) from 30 to 300 K[22]. The comparisons between the published data and the measured data are arranged and shown in Table 1. The published data in the literature showed the TOC at $\lambda = 1200$ nm of the fused silica material (Corning 7980). The test data is the effective TOC of the modes in the FBG core. The two values are different numerically, but the change rules for the temperatures are the same[20]. So at each temperature point, the difference between the test data and published data is nearly 2.1×10^{-6}. After linearly fitting the data, the slopes of the test data fitted curve and the published data fitted curve are 2.81×10^{-8} and 2.78×10^{-8}, respectively. So the test results seemed to accord well with the literature work. But in other works, the test sample is much larger and the test method is much more

Table 1. Comparisons of the Measured Data and the Published Data

Temperature (K)	TOC of Fused Silica (Corning 7980) (Published Data)	TOC of Optical Fiber (Measured in the Study)
50	1.98×10^{-6}	0.11×10^{-6}
100	3.36×10^{-6}	1.24×10^{-6}
160	5.02×10^{-6}	2.82×10^{-6}
200	6.12×10^{-6}	4.00×10^{-6}
240	7.22×10^{-6}	5.29×10^{-6}
275	8.19×10^{-6}	6.50×10^{-6}

complicated compared with our test. Furthermore, to ensure the performance of the hybrid sensor, the measurement should be repeated several times and a good repeatability could be obtained. Further efforts should be made to enhance the device's sensitivity by optimizing the sensor structure.

In conclusion, a hybrid FFPI-FBG sensor fabricated by an etching method is demonstrated. The temperature characteristics of the sensor are experimented with from 273 to 30 K. The temperature response agrees well with the previous studies on the room temperature. The experimental results demonstrate that the CTE of fused silica is negative for all temperatures below approximately 220 K due to the transverse thermal motion of oxygen. Based on the analysis of the experimental data, we get the proposed formula for the CTE and TOC of a silica-based optical fiber at cryogenic temperatures. At the same time, the paper also compares its results with others, which also shows the superiority of this method.

This work was supported by the National High Technology Research and Development Program (No. 2012AA041203) and the National Natural Science Foundation of China (No. 61307099)

References

1. Y. Rao, Opt. Lasers Eng. **31**, 297 (1999).
2. G. Tang, J. Wei, W. Zhou, R. Fan, M. Wu, and X. Xu, Chin. Opt. Lett. **12**, 090604 (2014).
3. S. Yang, H. Sun, L. Yuan, X. Zhang, L. Zhou, and M. Hu, Chin. Opt. Lett. **11**, 120604 (2013).
4. S. W. James, R. P. Tatam, A. Twin, M. Morgan, and P. Noonan, Meas. Sci. Technol. **13**, 1535 (2002).
5. Z. Guo, J. Feng, and H. Wang, Cryogenics **52**, 10 (2012).
6. Saidi Parne, Microwave Opt. Technol. Lett. **53**, 5 (2011).
7. J. Li, H. Neumann, and R. Ramalingam, Cryogenics, **68**, 36 (2015).
8. M. Esposito, S. Buontempo, A. Petriccione, M. Zarrelli, G. Breglio, A. Saccomanno, Z. Szillasi, A. Makovec, A. Cusano, A. Chiuchiolo, M. Bajko, and M. Giordano, Sen. Actuators A **2**, 189 (2013).
9. Y. H. Kim, S. J. Park, S. W. Jeon, S. Ju, C. S. Park, W. T. Han, and B. H. Lee, Opt. Express **20**, 23744 (2012).
10. C. L. Lee, H. Y. Ho, J. H. Gu, T. Y. Yeh, and C. H. Tseng, Opt. Lett. **40**, 4 (2015).
11. L. Li, X. Tong, C. Zhou, and H. Wen, Opt. Commun. **284**, 1612 (2011).
12. H. Singh and J. Sirkis, J. Lightw. Technol. **15**, 647 (1997).
13. S. H. Aref, H. Latifi, M. I. Zibaii, and M. Afshari, Opt. Commun. **269**, 322 (2007).
14. Y. Rao, X. Zeng, Y. Zhu, Y. Wang, T. Zhu, Z. Ran, S. Yuan, and D. Liang, Acta Opt. Sin. **22**, 85 (2002).
15. K. Li and Z. Zhen, Chin. Opt. Lett. **7**, 3 (2009).
16. Y. Rao and Z. Ran, Opt. Fiber Technol. **19**, 808 (2013).
17. Q. Han, X. Zhao, F. Tu, and J. Luo, *Asia-Pacific Optical Communications* (International Society for Optics and Photonics, 2006).
18. S. Takahashi, J. Non-Cryst. Solids **30**, 3 (1979).
19. K. O. Hill and G. Meltz, J. Lightwave Technol. **15**, 8 (1997).
20. Y. J. Kim, Opt. Lett. **27**, 15 (2002).
21. M. P. Attfield, Chem. Commun. **5**, 5 (1998).
22. D. Leviton, "Temperature-dependent absolute refractive index measurements of synthetic fused silica," *Optomechanical Technologies for Astronomy*, 2006.